

## Mechanics of intermediate filament networks assembled from keratins K8 and K18†

Cite this: *Soft Matter*, 2013, **9**, 8871

Paul Pawelzyk,<sup>a</sup> Harald Herrmann<sup>b</sup> and Norbert Willenbacher<sup>\*a</sup>

We have investigated intermediate filament networks assembled from the recombinant keratins K8 and K18 *in vitro* at various protein and MgCl<sub>2</sub> concentrations using mechanical rheometry. Experimental parameters were chosen such that artifacts from sample surface elasticity or wall slip were avoided, and the gap width did not affect network formation. The modulus  $G_0$  depends weakly on the protein concentration ( $G_0 \sim c^{0.5}$ ) and the critical deformation  $\gamma_{\text{crit}}$  at which non-linear response sets in is concentration independent. These findings can be rationalized assuming that the cross-link density decreases with decreasing protein concentration, while the filament contour length between cross-links remains unchanged. Thus, filaments are more stretched at lower protein concentrations and this increase in conformational energy partly compensates the free energy decrease related to the change in cross-link density.  $G_0$  is independent of the MgCl<sub>2</sub> concentration indicating that the contribution of stretched filaments decreases when the cross-link density increases. Networks rupture when a critical strain is exceeded, but fully recover within 30 minutes. The non-linear network response is characterized by pronounced strain stiffening with increasing shear stress  $\sigma$ . Reduced differential modulus  $K'$  data obtained at different protein or MgCl<sub>2</sub> concentrations collapse onto a master curve. Two scaling regimes  $K' \sim \sigma^\alpha$  are observed with  $\alpha = 1$  at intermediate and  $\alpha = 0.6$  at high stresses. These exponents may be rationalized in terms of the glassy wormlike chain model assuming sticky contacts with finite, constant bond strength. Two distinct scaling regimes could also result from the existence of two types of filament contacts with different bond energies or by the compliance of individual filaments.

Received 23rd July 2013  
Accepted 26th July 2013

DOI: 10.1039/c3sm51999f

[www.rsc.org/softmatter](http://www.rsc.org/softmatter)

### Introduction

In metazoan cells, the cytoskeleton provides the stability to withstand external mechanical stress. At the same time, cells need to be highly flexible for essential cell functions such as crawling, invasion and division. The underlying mechanical properties exhibited by cells are brought about by three distinct types of intracellular filaments: F-actin, intermediate filaments (IFs) and microtubules. While microtubules and microfilaments consist only of the highly conserved protein tubulin and actin, respectively, the IF protein family includes 65 different cell specific members.<sup>1</sup>

Keratins constitute the most diverse subgroup of IF proteins. According to their biochemical properties they can be further distinguished into acidic (type I) and basic (type II) keratins. With respect to their biochemical function, they are distinguished as “soft” and “hard”, the former being expressed within cells and the later constituting appendages like hair and nails.<sup>2,3</sup>

Soft keratins are found almost exclusively in epithelial cells that line external and internal surfaces of the body. Basic and acidic keratin proteins form obligate heterodimers that further associate into tetrameric complexes *in vitro*, from which filaments with a characteristic diameter of 10 nm can be assembled.<sup>4–6</sup> Keratin 8 (K8) and keratin 18 (K18) are typically found in one-layered, “simple” epithelia that line the digestive, respiratory, and urogenital tracts.

Because of the complex, heterogeneous structures formed by IFs in many cells and because of the presence of associated, “cross-bridging” proteins such as plakins, the study of reconstituted networks *in vitro* has distinct advantages.<sup>7</sup> This approach allows us to study simplified model networks under well-defined buffer conditions using classical rheometry and to validate the applicability of polymer network models. As a characteristic parameter for single filaments, the persistence length  $l_p$  of several types of IFs has been determined: it ranges from 1  $\mu\text{m}$  for vimentin<sup>8</sup> to 0.3  $\mu\text{m}$  for K8/K18 filaments.<sup>5</sup> Hence, IFs are much more flexible than F-actin ( $l_p \approx 17 \mu\text{m}$ ).<sup>9</sup> In addition, IFs have very different biochemical properties. Nevertheless, both types of filaments exhibit several similarities with regard to the mechanical response of their networks.<sup>10–12</sup> For example, the mechanical properties of vimentin and neurofilaments in the presence of MgCl<sub>2</sub> exhibit characteristics

<sup>a</sup>Institute for Mechanical Process Engineering and Mechanics, Karlsruhe Institute of Technology, Gotthard-Franz-Straße 3, 76131 Karlsruhe, Germany. E-mail: [norbert.willenbacher@kit.edu](mailto:norbert.willenbacher@kit.edu)

<sup>b</sup>Division of Molecular Genetics, Cancer Research Center (DKFZ), Heidelberg, Germany

† Electronic supplementary information (ESI) available. See DOI: 10.1039/c3sm51999f

comparable to those shown by cross-linked actin networks.<sup>12,13</sup> However, keratin filaments assemble quite differently from these two types of IF proteins, both with respect to the assembly kinetics and the ionic requirements for assembly.<sup>5,14</sup> Hence, it is important to investigate how this distinct behavior translates to the network mechanics.

Rheological studies on the bulk properties of keratin networks reveal only a very weak influence of the protein concentration on network elasticity in the linear viscoelastic regime at small deformations.<sup>15,16</sup> This behavior cannot be explained by the theoretical concepts for networks of semi-flexible polymers with a persistence length similar to the contour length.<sup>10,17,18</sup> For K8/K18, the weak influence of the protein concentration on elasticity was assigned to the contribution of the air–liquid interface at the open rheometer fixture.<sup>15</sup> Here we show that this explanation does not hold for networks assembled from K8/K18 and that the weak concentration dependency can be explained by the theoretical concept for swollen networks of a chemically cross-linked flexible polymer.

Another prominent feature of cytoskeletal protein filament networks is their non-linear stiffening behavior at large deformations or stresses.<sup>12,13,19–23</sup> The nonlinear properties of K8 and K18 were already studied using standard large amplitude oscillatory shear (LAOS).<sup>15</sup> This study revealed no strain stiffening of K8/K18 at physiological pH values. At the maximum deformation the network ruptures. We utilized the LAOS method to probe the recovery of the network after disruption. For quantitative characterization of the non-linear properties we used the differential modulus obtained from superposition of a small amplitude oscillatory shear stress and a larger steady pre-stress.<sup>11,24</sup> Thereby we have studied the impact of both protein and divalent cation concentrations on the linear and non-linear mechanical bulk properties of the networks. These rheological studies were combined with structural investigations of such networks using scanning electron microscopy (SEM) and multiple particle tracking (MPT).

## Materials and methods

Human K8 and K18 were expressed and purified as described.<sup>25</sup> 1 : 1 mixtures of K8 and K18, dissolved in 8 M urea and 10 mM Tris–HCl (pH 7.5), were renatured by dialysis against 8 M urea, 2 mM Tris–HCl (pH 9.0) and 1 mM DTT with stepwise reduction of the urea concentration (6 M, 4 M, 2 M) to urea-free 2 mM Tris–HCl (pH 9.0) buffer containing 1 mM DTT. The protein concentration was determined by a Bradford assay (Bio-Rad) using bovine serum albumin as the standard. The assembly was started by addition of an equal volume of assembly buffer (ASB) consisting of 18 mM Tris–HCl (pH 7.0) and 0–3 mM MgCl<sub>2</sub>, resulting in a final buffer condition of 10 mM Tris–HCl (pH 7.4) and 0–1.5 mM MgCl<sub>2</sub>. The mixtures were assembled for 60 min at 20 °C between the rheometer plates.

For SEM imaging, the keratin solutions were mixed with 2.5 μl dispersion of 1 μm PS microspheres (Thermo Scientific, Duke Standards) in ddH<sub>2</sub>O at a concentration of 10% prior to assembly. The assembled protein networks were fixed with

glutaraldehyde, critical point dried, platinum coated, and imaged as described by Leitner *et al.*<sup>26</sup> When the three-dimensional network collapses after dehydration, the filaments settle on the glass substrate and the polystyrene beads. The filaments between the beads and the glass substrate, which are not attached to a surface, provide a good impression of the network.

For the MPT experiments, we used green fluorescent polystyrene tracer particles (Bangs Laboratories, USA) with a diameter of 0.52 μm or 1.01 μm and different surface functionalities. Unfunctionalized particles were used as supplied. The PEG functionalized particles were coated according to the swelling based approach of Kim and co-workers<sup>27</sup> using Pluronic F127. The particles dispersed in dialysis buffer were mixed with the protein solution by vortexing to obtain a final particle concentration of 0.01%. After addition of the assembly buffer, both solutions were mixed and filled in a self-build sample chamber, which was sealed using an UV curing optical adhesive (NOA63, Norland Optical Adhesive, USA). The size of the sample chamber was 5 × 10 mm with a thickness of 160 μm. The particles were tracked at a temperature of 20 °C using an inverted fluorescence microscope (Zeiss Axiovert 200) with a C-Apochromate 40× objective and a CCD camera (Pike F100-B or Stingray F033B, Allied Vision Technologies, Germany) at a speed of 30 frames per second and at resolutions below 0.15 μm per pixel. For each measurement, 5 sets of 300 s at randomly chosen positions were recorded. Each measurement comprises between 37 and 135 particles. The images were processed and analyzed as previously described.<sup>28</sup>

LAOS experiments were conducted using a RheoScope 1 (Thermo Fisher Scientific, Karlsruhe, Germany) equipped with a cone–plate geometry (diameter: 35 mm, cone angle: 1°). The linear viscoelastic properties and the differential modulus were measured on a Physica MCR 501 (Anton Paar, Graz, Austria). Plates with 25 and 50 mm diameter were used and the gap width was varied between 0.12 mm and 1.2 mm. A solvent trap was used to minimize evaporation of water. For long measurements at a low gap width, the surface was additionally coated with low viscosity paraffin oil. The elastic modulus  $G' = (\hat{\alpha}/\hat{\gamma})\cos \delta$  and the viscous modulus  $G'' = (\hat{\alpha}/\hat{\gamma})\sin \delta$  were obtained by application of a sinusoidal strain with amplitude  $\hat{\gamma}$  and measurement of the resulting stress amplitude  $\hat{\alpha}$  and phase shift  $\delta$ . The frequency dependence of  $G'$  and  $G''$  was measured at  $\hat{\gamma} = 1\%$ . This deformation is within the linear response regime according to preliminary amplitude sweep experiments. LAOS experiments were conducted in the stress-controlled mode at a frequency of 1 rad s<sup>-1</sup>. The differential modulus  $K'$  was measured by pre-stressing the sample with a steady stress  $\sigma_0$  for 2 min and superposition of a small oscillatory stress  $\partial\sigma \leq 0.1\sigma_0$  at  $\omega = 6.3$  rad s<sup>-1</sup>. The complex differential or tangential modulus is given by  $K^*(\omega, \sigma_0) = \partial\sigma/\partial\gamma$ .

## Results and discussion

### Network structure

SEM images and MPT experiments of K8/K18 networks at different protein and MgCl<sub>2</sub> concentrations at 0.5 g l<sup>-1</sup> K8/K18 were used to assess the network structure (Fig. 1).

The micrograph representing a K8/K18 network at  $0.1 \text{ g l}^{-1}$  (Fig. 1a) shows no space filling network as only few filaments were found between the beads and the substrate. Most filaments, however, lay on the glass substrate. The networks encountered at a protein concentration of  $0.5 \text{ g l}^{-1}$  and  $\text{Mg}^{2+}$  concentrations between  $0.5$  and  $1.0 \text{ mM}$  (Fig. 1b, d and e) appear fairly homogeneous and resemble the filaments in epithelia cells as shown by Leitner *et al.*<sup>26</sup> The filaments on SEM images seem to be more stretched as on transmission electron micrographs from highly diluted filament solutions.<sup>5</sup> This may reflect a stretched filament conformation in the network or may be an artifact from sample preparation. SEM images at a protein concentration of  $1.0 \text{ g l}^{-1}$  (Fig. 1c) and  $0.5 \text{ g l}^{-1}$  protein in combination with  $1.5 \text{ mM MgCl}_2$  (Fig. 1f) show mainly bundled filaments with some single filaments as concluded from the apparent filament diameters. Whether these bundled filaments are characteristic for these networks or just an artifact from sample preparation will be discussed below in the light of the results from MPT experiments.

The MPT experiments characterize the homogeneity of the networks in their natural aqueous environment.<sup>29</sup> The diffusive motion of tracer particles from MPT experiments is characterized by their mean square displacement (MSD). At a protein concentration of  $0.1 \text{ g l}^{-1}$  the MSDs of particles with a diameter

of  $1.01 \mu\text{m}$  increase linearly with time, *i.e.* the particles diffuse freely in a purely viscous environment (Fig. 1A). Therefore, we conclude that the mesh size  $\xi$  is larger than  $1.01 \mu\text{m}$ . This is consistent with an estimate of the mesh size assuming a cubic grid of rigid filaments:

$$\xi = \sqrt{3/\rho} \quad (1)$$

with the length density of the filament  $\rho = c/\lambda$  calculated from the mass per unit length  $\lambda = 19 \text{ kDa nm}^{-1} = 3.16 \times 10^{-11} \text{ g m}^{-1}$  for K8/K18.<sup>25</sup> For a  $0.1 \text{ g l}^{-1}$  K8/K18 solution this results in  $\xi = 0.97 \mu\text{m}$ . At K8/K18 concentrations of  $0.5 \text{ g l}^{-1}$  the MSDs approach a constant value indicating that the particles are trapped in an elastic environment (Fig. 1B). Consistently, the mesh size estimated from eqn (1) is  $\xi = 0.435 \mu\text{m}$ , which is significantly smaller than the particle diameter. The addition of  $\text{MgCl}_2$  decreases the magnitude and slope of the MSDs (Fig. 1D–F) indicating that the network becomes stiffer upon addition of divalent ions. Moreover, the distribution of MSD values at a given lag time  $\tau$  broadens with increasing  $\text{MgCl}_2$  concentration demonstrating that the network inhomogeneity increases when salt is added. In contrast, the distribution of MSD values is fairly narrow for the samples without added salt independent of the protein concentration.

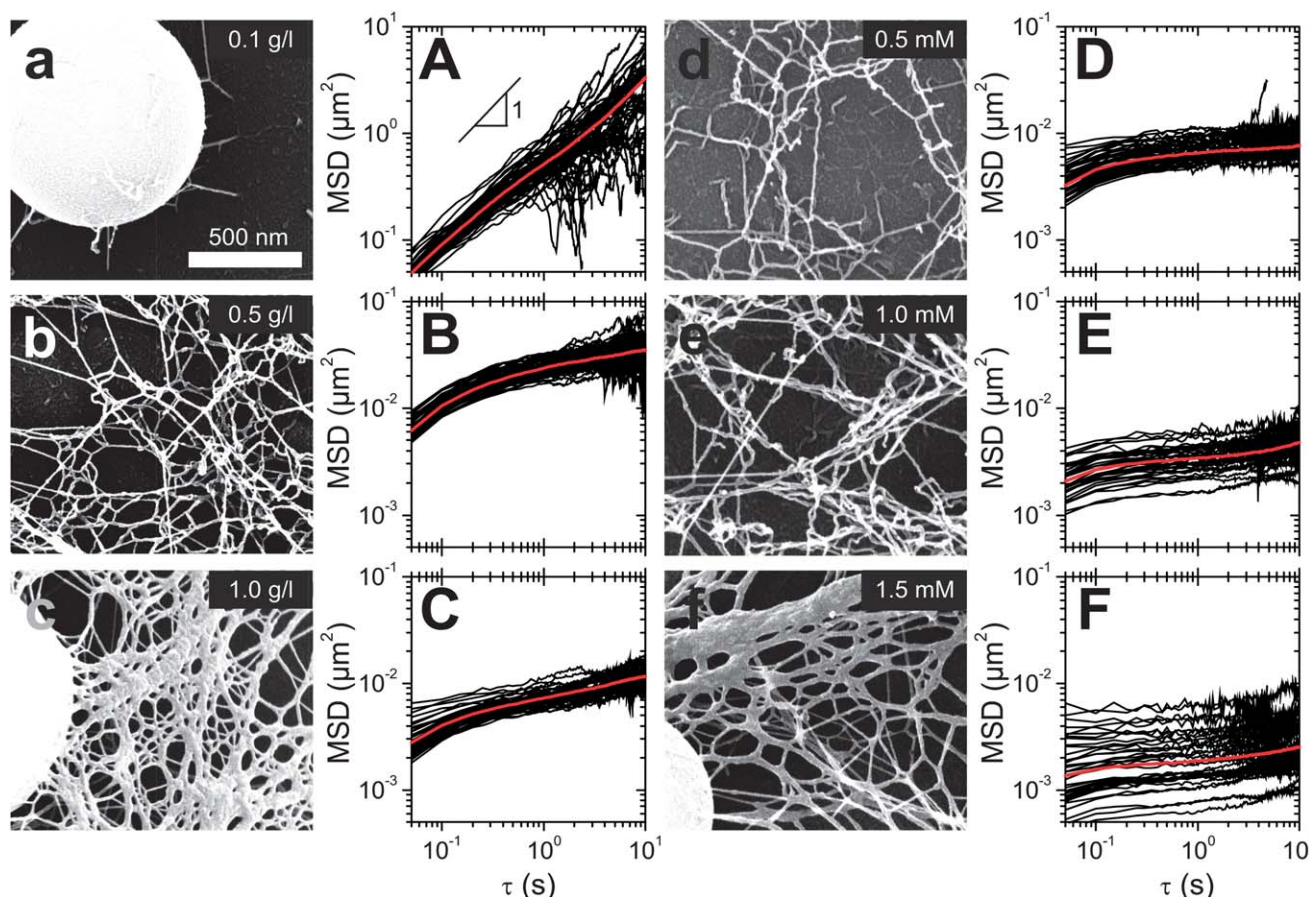


**Fig. 1** SEM images (small letters) and MSDs of  $1.01 \mu\text{m}$  PEG coated particles (capital letters) of K8/K18 networks without salt at different protein concentrations (a–c) and at different  $\text{MgCl}_2$  concentrations and a protein concentration of  $0.5 \text{ g l}^{-1}$  (d–f). Scale bar is the same for all panels.

To analyze the heterogeneity of the samples quantitatively we calculated the non-Gaussian parameter  $\alpha_2$ .<sup>30</sup> The parameter compares the fourth and the second moment of the distance  $\Delta x(\tau)$  a particle travels within the time interval  $\tau$ :

$$\alpha_2 = \frac{\langle \Delta x(\tau)^4 \rangle}{3 \langle \Delta x(\tau)^2 \rangle^2} - 1. \quad (2)$$

The  $\alpha_2$ -parameter is zero for a Gaussian distribution of MSDs expected for homogeneous samples and increases with increasing inhomogeneity of the environment explored by the tracer particles. Fig. 2 shows the results from five independent experiments with different particle diameters and different surface functionalities at an interval lag time of  $\tau = 1$  s. The results show that the heterogeneity increases with protein but even more with  $\text{Mg}^{2+}$  concentration. The heterogeneity of the sample with  $1.0 \text{ g l}^{-1}$  K8/K18 is similar to the sample with  $0.5 \text{ g l}^{-1}$  K8/18 at a  $\text{MgCl}_2$  concentration of  $0.5 \text{ mM}$ , which clearly shows no bundling in SEM images (Fig. 1d). Generally, bundling results in an inhomogeneous network structure.<sup>31,32</sup> Since the  $\alpha_2$  values for the salt-free protein networks are close to zero, we assume that the bundling for the  $1.0 \text{ g l}^{-1}$  K8/K18 sample appearing in Fig. 1c is an artifact from sample preparation.

### Linear network response

The qualitative evolution of the moduli during assembly and network formation is similar to desmin and vimentin (Fig. S1 in the ESI†).<sup>20</sup> The absolute modulus value of  $G'$  is about a factor of three higher for K8/K18 compared to vimentin at a similar filament length density.  $G'$  is larger than  $G''$  even for the first data point taken about 1 min after closing the rheometer gap. Although the moduli quickly change in this initial period, this suggests that a network may have already existed when the gap closes and this network is exposed to an initial deformation

prior to our rheological characterization. The influence of the protein and the  $\text{MgCl}_2$  concentration on the network response in the linear viscoelastic regime is shown in Fig. 3. All samples exhibit predominantly elastic behavior in the frequency range between  $0.01$  and  $25 \text{ rad s}^{-1}$ , *i.e.*  $G' \gg G''$ . Moreover,  $G'$  is approximately frequency independent and its absolute value is termed the plateau modulus  $G_0$ . In the following  $G_0$  is defined as the  $G'$  value obtained at  $\omega = 6.3 \text{ rad s}^{-1}$ . The dissipation factor  $\tan \delta = G''/G'$  of all samples is between  $0.1$  and  $0.2$ . This gel-like behavior is typical for chemically or physically cross-linked polymer networks. Obviously, such a network exists even at a protein concentration as low as  $0.1 \text{ g l}^{-1}$  for which SEM and MPT data do not indicate such a structure.

Small amplitude oscillatory shear experiments were performed using different setups in order to judge the effect of experimental artifacts or secondary flow phenomena. First, we have changed the diameter of the rheometer plate from  $50 \text{ mm}$  to  $25 \text{ mm}$  at a constant gap width of  $0.12 \text{ mm}$ . As a consequence, the ratio of the air-liquid interface to the sample volume increases by a factor of two. If the elasticity of the air-liquid interface would contribute significantly to the apparent bulk rheological properties as reported by Yamada *et al.*<sup>15</sup> the modulus should increase with decreasing plate diameter. These authors further proposed to suppress the effect by coating the surface with the phosphor lipid *1,2-dimyristoyl-rac-glycero-3-phosphocholine* in chloroform. Fig. 4 shows that such surface effects are obviously not relevant here as the  $G_0$  data obtained with different geometries and different surface treatment agree well within experimental error. Next, we have changed the gap width from  $0.12 \text{ mm}$  to  $1.2 \text{ mm}$  at a constant plate diameter of  $25 \text{ mm}$ , *i.e.* the sample volume changes from  $70 \mu\text{l}$  to  $600 \mu\text{l}$ . Again no significant effect on the resulting modulus data is observed. The load on the sample while squeezing the droplet into the rheometer gap and the time to fill the rheometer gap

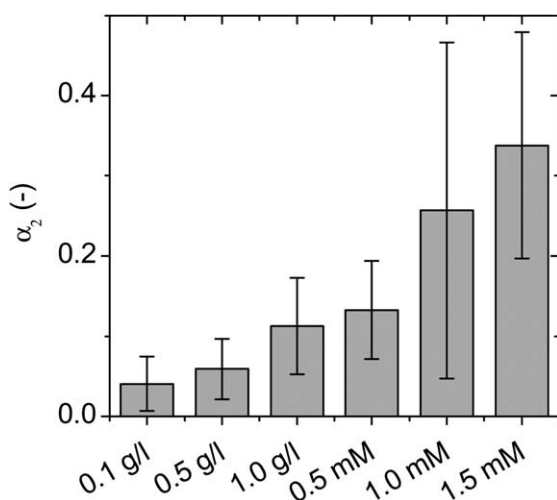


**Fig. 2** Heterogeneity of the networks measured by the non-Gaussian parameter  $\alpha_2$  at a time interval of  $\tau = 1$  s for samples with different K8/K18 concentrations and for samples with different  $\text{MgCl}_2$  concentrations at a fixed K8/K18 concentration of  $0.5 \text{ g l}^{-1}$ .

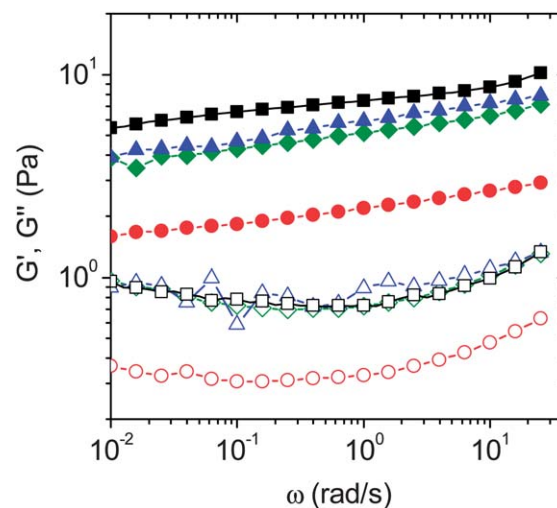


**Fig. 3** Frequency dependency of the storage modulus  $G'$  (closed symbols) and the viscous modulus  $G''$  (open symbols) in the linear viscoelastic regime of K8/K18 filaments at concentrations of  $0.1 \text{ g l}^{-1}$  (circles),  $0.5 \text{ g l}^{-1}$  (diamonds),  $0.5 \text{ g l}^{-1}$  with  $1.5 \text{ mM MgCl}_2$  (triangles), and  $1.0 \text{ g l}^{-1}$  (squares).

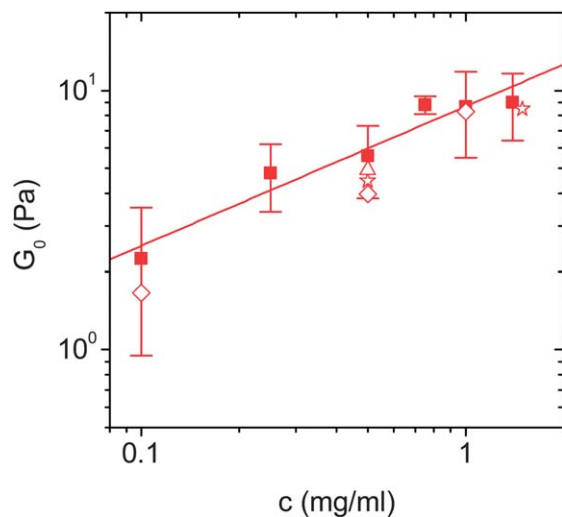


**Fig. 4** The plateau modulus  $G_0$  versus K8/K18 concentration. Measurements were conducted at a frequency of  $6.3 \text{ rad s}^{-1}$  with a 50 mm plate with a 0.12 mm gap (squares), with a 25 mm plate with a 0.12 mm gap (open diamonds), with a 25 mm plate and a 1.2 mm gap (open stars), and K8/K18 with phosphor lipid coating (open triangle). The red line illustrates a scaling of  $G_0 \sim c^{7/12}$ .

increase drastically with decreasing gap width. Obviously, this has no significant effect on the subsequent assembly and network formation. This is particularly remarkable since K8/K18 assembles more than 80 times faster than *e.g.* vimentin.<sup>5</sup> Furthermore, measuring the shear moduli could be affected by wall slip. Then the apparent moduli should decrease with decreasing gap width, but the data shown in Fig. 4 do not indicate that this phenomenon is relevant here. The dependence of the plateau modulus  $G_0$  on the keratin concentration is weak and can be described by a power law  $G_0 \sim c^x$  with  $x = 0.5 \pm 0.08$ .

Different theoretical models have been proposed in the literature to describe the relationship between  $G_0$  and the microscopic network and filament features. The relevant length scale in all these models is in the range of the mesh size or the length between adjacent cross-links, which are related to the cross-link density of the network. The tube model for entangled semiflexible polymers predicts a  $G_0 \sim c^{1.4}$  scaling.<sup>17</sup> This model has been used to explain the scaling of entangled actin solutions,<sup>17</sup> neurofilaments,<sup>23</sup> and vimentin at high concentrations.<sup>13</sup> The worm-like chain model results in a scaling of  $G_0 \sim c^2$  for cross-linked networks of semiflexible or rod-like polymers or a  $G_0 \sim c^{5/3}$  scaling in the “snakelike” regime.<sup>18</sup> The MacKintosh model discusses  $G_0$  in terms of thermal fluctuation of single semiflexible filaments between adjacent cross-links or entanglements. The model results in a scaling of  $G_0 \sim c^{2.2}$  for an entangled network of a semiflexible polymer and in  $G_0 \sim c^{2.5}$  for cross-linked rods.<sup>10</sup> This scaling was observed for vimentin and neurofilaments in the presence of divalent ions, which exhibit values of  $x = 2.0$  and  $x = 2.5$ , respectively.<sup>12</sup>

The weak increase of  $G_0$  with protein concentration found for K8/K18 cannot be explained by any of these models. However studies on intermediate filament networks from K5/K14,<sup>16</sup> vimentin,<sup>16,19,20</sup> desmin<sup>20</sup> and K8/K18 (ref. 15) without

treatment of the air–liquid interface by phospholipids found the same weak effect of protein concentration on the plateau modulus. The exponents in these investigations are ranging from  $x = 0.25$  for untreated K8/K18 (ref. 15) to  $x = 0.70$  for desmin.<sup>20</sup> The inconsistency with theoretical models was explained by structural changes of the network (*e.g.* bundling),<sup>20</sup> attractive filament–filament interactions<sup>16,33</sup> or strong elasticity of the air–liquid interface.<sup>15</sup> The latter can be excluded here as discussed above. SEM images and MPT experiments show no clear indication for bundling to occur in networks without added salt. Furthermore, bundling would result in  $G_0$  values at high protein concentrations lower than expected for networks of individual filaments. Instead, the weak concentration dependence of the modulus observed here is a consequence of the high  $G_0$  values found at low protein concentrations. The experimental data are much higher than the corresponding values for entangled actin solutions at similar length densities.<sup>17,34</sup> The plateau modulus  $G_0$  can be directly calculated from the mesh size  $\xi$  using the classical theory for rubber elasticity:<sup>35</sup>

$$G_0 = \frac{k_B T}{\xi^3} \quad (3)$$

with the Boltzmann constant  $k_B$  and the temperature  $T$ . From our MPT experiments at  $0.1 \text{ g l}^{-1}$  protein concentration we can estimate  $\xi \geq 1 \mu\text{m}$ . According to eqn (3) this corresponds to  $G_0 \leq 4 \times 10^{-3} \text{ Pa}$ . For an affine deformation of semi-flexible polymers in a network the modulus can be assessed from the length density  $\rho$ , the persistence length  $l_p$  and the contour length of the filament between adjacent cross-links  $l_c$ :<sup>12</sup>

$$G_0 = 6 \rho k_B T \frac{l_p^2}{l_c^3}. \quad (4)$$

The persistence length of K8/K18 (ref. 5) is  $l_p = 0.3 \mu\text{m}$  and  $l_c$  is equal to or larger than  $\xi$ . For a K8/K18 concentration of  $0.1 \text{ g l}^{-1}$  and a mesh size of  $\xi = 1 \mu\text{m}$  the model results in  $G_0 \leq 2 \times 10^{-3} \text{ Pa}$ . The deviation between measured data and these model predictions decreases with increasing protein concentration. Therefore, we have to conclude that there must be an additional contribution to the free energy of the network to account for the high moduli at low protein concentrations. Inspired by the classical theory describing the swelling of chemically cross-linked networks of flexible polymer chains we propose an additional contribution from stretched filaments between cross-links. For such networks the cross-link density decreases upon swelling, but the contour length of network strands between adjacent cross-links  $l_c$  is constant. The weak influence of the polymer concentration on  $G_0$  is a consequence of two competing effects. The cross-link density decreases with decreasing polymer concentration, but this is partly compensated by stretching of polymer strands associated with an increase in conformational free energy. This theory predicts  $G_0 \sim c^{1/3}$  for a polymer network in a  $\theta$ -solvent and  $G_0 \sim c^{7/12}$  in a good solvent.<sup>36</sup> The latter scaling law is in excellent agreement with our experimental observations shown in Fig. 4. Therefore, we hypothesize that the number of cross-links in the K8/K18 networks investigated here is approximately independent of the

protein concentration and that the filament strands between cross-links are more stretched at lower concentrations. This explains not only the weak concentration dependency of  $G_0$ , but also the high modulus values at low protein concentrations. The model indicates that the stretched filaments on the SEM images in Fig. 1 represent the natural filament conformation within the network.

The effect of added  $\text{MgCl}_2$  on  $G_0$  at a constant K8/K18 concentration is shown in Fig. 5. Obviously, the  $\text{MgCl}_2$  concentration does not affect the network modulus indicating that the cross-link density is independent of the  $\text{MgCl}_2$  concentration. In contrast, Lin and co-workers have observed a scaling of  $G_0 \sim R^{0.6}$  for vimentin and neurofilaments, where  $R$  is the ratio of the molar concentrations of divalent ions to IF proteins.<sup>12</sup> The moduli of K8/K18 obtained from micro-rheological experiments<sup>26</sup> increase even stronger with increasing  $\text{MgCl}_2$  concentration. But calculation of the bulk modulus of a gel or network sample from MPT results is based on the assumption that the tracer particles move in a homogeneous continuum, *i.e.* the MSD data show a Gaussian distribution with  $\alpha_2 \approx 0.37$ . This is not the case here when salt is added and therefore we cannot compare our macroscopic data with the results of Leitner *et al.*<sup>26</sup> Nevertheless, quantitative analysis of SEM images<sup>26</sup> also suggest that the mesh size decreases with increasing  $\text{MgCl}_2$  concentration. As shown above, the bulk moduli include a contribution from strong non-equilibrium stretching of filaments between cross-links. This contribution decrease with increasing cross-link density seems to balance the contribution of increasing cross-link density upon addition of  $\text{MgCl}_2$ .

### Nonlinear network response

Biological networks rupture when a critical maximum strain  $\gamma_{\text{max}}$  is exceeded. First, we characterize how this disruption affects the network properties of K8/K18 filaments by three

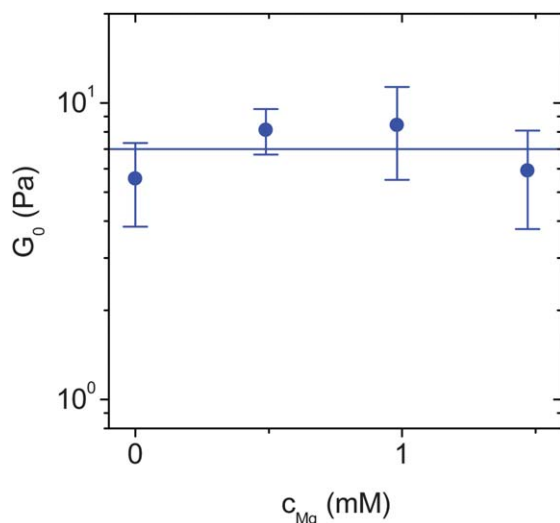


**Fig. 5**  $G_0$  at a frequency of  $6.3 \text{ rad s}^{-1}$  versus  $\text{MgCl}_2$  concentration at a K8/K18 concentration of  $0.5 \text{ g l}^{-1}$ .

consecutive LAOS experiments. Fig. 6 shows the apparent storage modulus  $G'$  normalized by  $G'$  of the mature network after 60 min of assembly. In the first run, the stress amplitude was increased from 0.01 to 10 Pa. The maximum in the strain amplitude was chosen such that the critical strain  $\gamma_{\text{max}} \approx 1.1$  at which the network ruptures was not reached. Accordingly, the shape of the curve plotting  $G'$  versus  $\gamma$  in the second run is essentially the same as in the first run until  $\gamma_{\text{max}}$  is reached. Then  $G'$  drops drastically, indicating the rupture of the network. It takes about 30 min for the network to recover and to reach its initial modulus value. The third amplitude sweep was directly started after  $G'$  had reached its initial value again. But note that the modulus has not reached a limiting value at this time. The inset in Fig. 6 reveals that the modulus would further increase if the waiting time was prolonged. This is also visible from the  $G'$  data characterizing the initial assembly and network formation kinetics (Fig. S1†) and should be addressed in future research efforts. The normalized  $G'$  data for the third run exhibit a similar functional form to the first run confirming the reconstitution of the network. Similar behavior has been observed for K5/K14 (ref. 16) and neurofilament networks.<sup>22</sup> In contrast, desmin filament networks are irreversibly damaged after exceeding the critical strain  $\gamma_{\text{max}}$  and do not recover within waiting times on the order of 30 to 60 min.<sup>20</sup>

LAOS experiments have been used recently to characterize strain stiffening for vimentin, desmin as well as keratin networks and proved that they are well suited for qualitative comparison.<sup>20,21</sup> The interpretation of data and a rigorous comparison to theory, as *e.g.* the glassy worm like chain model, is difficult because the strain response becomes aperiodic and non-sinusoidal. Therefore, we examined the differential

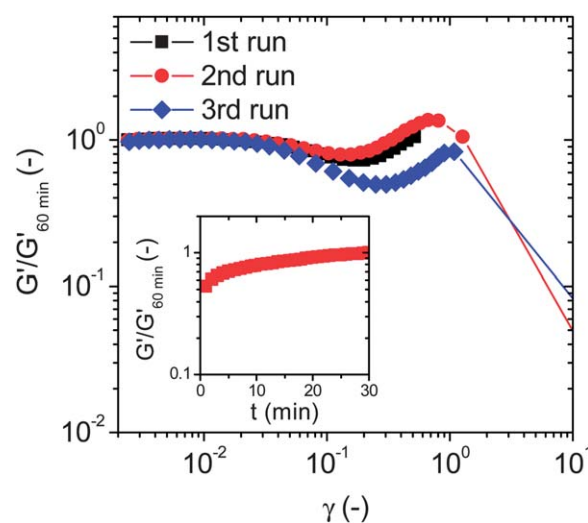


**Fig. 6** Deformation dependence of storage modulus  $G'$  normalized by  $G'$  determined after 60 min assembly time for a K8/K18 solution with  $c = 0.5 \text{ g l}^{-1}$  at a frequency of  $\omega = 1 \text{ rad s}^{-1}$ . The moduli are shown for three subsequent measurements on the same sample. In the first run the maximum strain amplitude was chosen such that the maximum in  $G'$  was not yet reached. In the second run,  $\gamma$  was increased until rupture of the sample occurred and the third run was performed after a recovery time of 30 min. Inset: recovery of the samples between the 2<sup>nd</sup> and the 3<sup>rd</sup> run measured at  $\dot{\gamma} = 1\%$ .

modulus  $K'$  to characterize the nonlinear viscoelastic network response. We have applied a constant pre-stress  $\sigma_0$  for 2 min and superimposed a small oscillatory stress  $\partial\sigma$ . From the resulting oscillatory strain amplitude  $\partial\gamma_0$  and phase shift  $\delta$  the differential storage modulus was calculated as  $K' = (\partial\sigma_0/\partial\omega_0) \cos \delta$ . The corresponding data for a K8/K18 concentration of  $0.5 \text{ g l}^{-1}$  are shown in Fig. 7. The measured signal increases at the beginning of each stress pulse, but after  $\sim 1$  min a steady state is reached and  $K'$  is evaluated. The data of  $K'$  as a function of pre-stress  $\sigma_0$  are shown in the inset. In the linear regime at low pre-stresses  $\sigma_0$  the differential modulus  $K'$  is constant and equals the plateau modulus  $G_0$ . After reaching a critical pre-stress  $\sigma_{\text{crit}}$  the network starts to stiffen. From the critical pre-stress the critical strain  $\gamma_{\text{crit}}$  can be calculated as  $\gamma_{\text{crit}} = \sigma_{\text{crit}}/G_0$ . The differential modulus increases until a maximum stress  $\sigma_{\text{max}}$  at which the network ruptures is reached. At this point the network reaches the highest elasticity  $K'_{\text{max}}$ .

Fig. 8 shows the influence of the protein concentration and the  $\text{Mg}^{2+}$  concentration on the critical deformation  $\gamma_{\text{crit}}$  where the non-linear response sets in. Obviously,  $\gamma_{\text{crit}} \approx 0.09$  is independent of the protein and  $\text{MgCl}_2$  concentrations. For semi-flexible filaments,  $\gamma_{\text{crit}}$  is directly proportional to the filament contour length between adjacent cross-links  $l_c$  if the elasticity is entropic in origin:

$$\gamma_{\text{crit}} = \frac{\sigma_{\text{crit}}}{G_0} \sim \frac{k_B T}{\kappa_0} l_c \quad (5)$$

with the Boltzmann constant  $k_B$  and the bending stiffness  $\kappa_0$ .<sup>10</sup> According to the results shown in Fig. 6,  $\gamma_{\text{crit}}$  and hence  $l_c$  are independent of the K8/K18 and the  $\text{Mg}^{2+}$  concentration assuming a constant  $\kappa_0$ . Since  $l_c$  is independent of protein concentration, the filament strands between cross-links must be stretched at lower protein concentrations. Accordingly, their conformational energy increases and this confirms the model

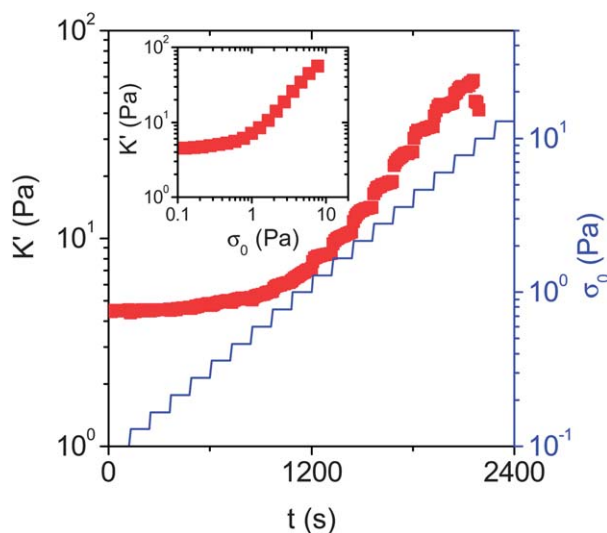


**Fig. 7** The differential storage modulus  $K'$  versus time at a constant frequency of  $\omega = 6.3 \text{ rad s}^{-1}$  and varying pre-stress  $\sigma_0$  at a K8/K18 concentration of  $0.5 \text{ g l}^{-1}$ .  $\sigma_0$  is stepwise increased from 0.1 to 10 Pa. The time interval for each step is 2 min. The inset shows  $K'$  as a function of  $\sigma_0$ .

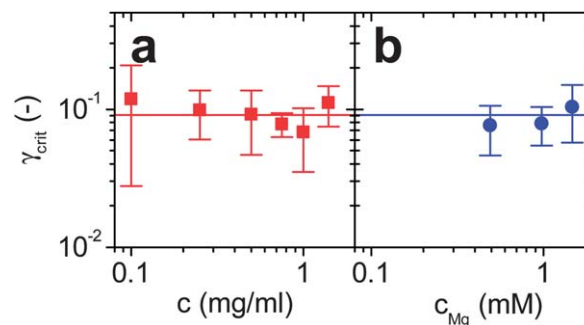


**Fig. 8** The influence of the K8/K18 concentration (a) and the  $\text{MgCl}_2$  concentration at a protein concentration of  $0.5 \text{ g l}^{-1}$  (b) on  $\gamma_{\text{crit}}$ .

presented above describing the weak dependency of  $G_0$  on protein concentration. In contrast,  $l_c$  decreases with protein concentration for vimentin and neurofilaments in the presence of divalent ions according to a power law  $l_c \sim c^{-0.4}$ , which is close to the scaling for the mesh size of a cubic grid of rigid filaments ( $\xi \sim c^{-0.5}$ ).<sup>12</sup> Moreover, a decrease of  $l_c$  with increasing  $\text{Mg}^{2+}$  concentration was found for these systems:  $l_c \sim c_{\text{Mg}}$  determined from  $\gamma_{\text{crit}}$ .<sup>12</sup> A scaling of  $l_c \sim c_{\text{Mg}}^{-0.39}$  was found for K8/K18 by quantitative analysis of SEM data.<sup>26</sup> However, the corresponding decrease in  $\gamma_{\text{crit}}$  is within the experimental uncertainty for the concentration range investigated here.

The influence of the protein concentration and the  $\text{Mg}^{2+}$  concentration on  $\sigma_{\text{max}}$  and  $K'_{\text{max}}$  is shown in Fig. 9. In contrast to the linear viscoelastic properties and  $\gamma_{\text{crit}}$ , both non-linear quantities strongly depend on protein and divalent ion concentration. According to Storm and co-workers,  $\sigma_{\text{max}}$  is mainly controlled by the strength of the bonds between filaments and  $K'_{\text{max}}$  by the strain stiffening mechanism and the compliance of filaments in an axial direction.<sup>38</sup>

The data for the differential modulus  $K'$  obtained at different protein and  $\text{Mg}^{2+}$  concentrations result in a master curve when  $K'$  is normalized by  $G_0$  and  $\sigma_0$  by  $\sigma_{\text{crit}}$  as demonstrated in Fig. 10. The corresponding raw data are shown as an inset. The non-linear response is characterized by two scaling regimes  $K' \sim \sigma_0$  with different exponents  $\alpha$ . At intermediate stresses the increase of  $K'$  is characterized by  $\alpha \approx 1.0$ . The scaling exponent  $\alpha \approx 0.6$  is found in the high stress regime.

Master curves for normalized  $K'$  versus  $\sigma_0$  data have also been found for other cytoskeletal filament networks but with different  $\alpha$ -values and different scaling regimes. Rammensee and colleagues found a single scaling regime with  $\alpha = 1$  for neurofilaments.<sup>23</sup> Actin and the rigid cross-linker scruin,<sup>11,39</sup> and neurofilaments with  $\text{MgCl}_2$  (ref. 12) as well, show only a single scaling regime, but with an  $\alpha$ -value of  $3/2$ . Vimentin<sup>12,13</sup> and actin cross-linked by the flexible cross-linker filamin<sup>40</sup> show a second regime at high stresses in addition to the  $\alpha = 3/2$  scaling at intermediate stresses. For vimentin,  $K'$  gradually levels off at high stresses, but actin cross-linked by filamin<sup>40</sup> shows a second regime with a constant slope of  $\alpha = 1$ . On the other hand actin solutions,<sup>41</sup> bundled actin-fascin networks<sup>42</sup> and actin isotropically cross-linked by heavy meromyosin<sup>43</sup> show  $\alpha$ -values, which depend significantly on parameters such

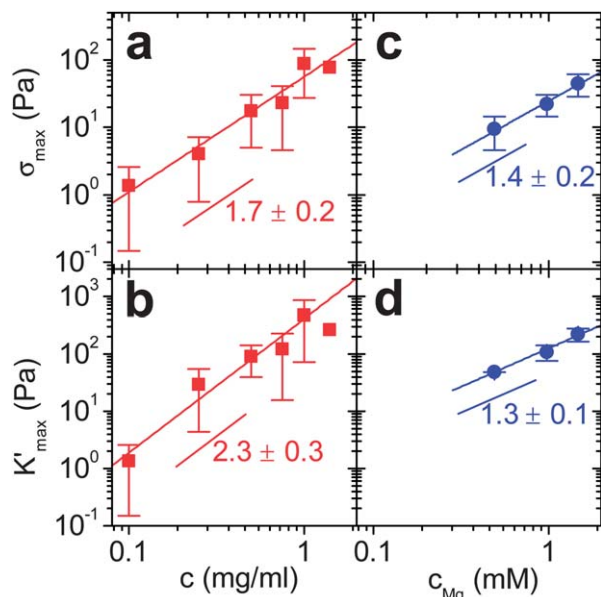


**Fig. 9** The stress at which the networks rupture  $\sigma_{\text{crit}}$  and the maximal elasticity  $K'_{\text{max}}$  of the network versus K8/K18 concentration (a and b) and versus  $\text{MgCl}_2$  concentration at a K8/K18 concentration of  $0.5 \text{ g l}^{-1}$  (c and d).

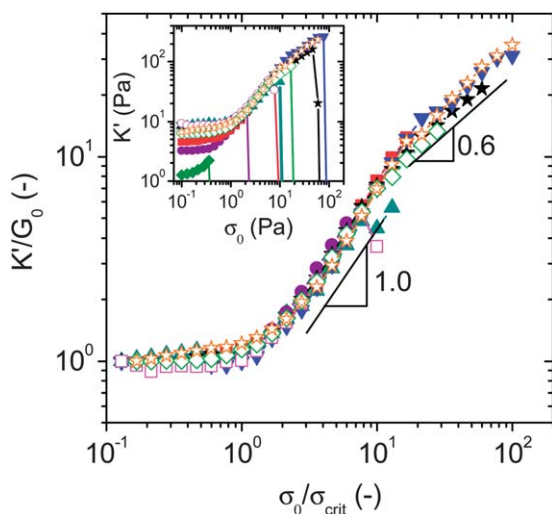


**Fig. 10**  $K'$  and  $\sigma_0$  normalized by  $G_0$  and  $\sigma_{\text{crit}}$ . Inset: raw data used for the master curve. Closed symbols correspond to K8/K18 concentrations of 0.1 (diamonds), 0.25 (circles), 0.5 (squares), 0.75 (up triangles), 1.0 (stars), and 1.4  $\text{g l}^{-1}$  (down triangles). Open symbols represent  $\text{MgCl}_2$  concentrations of 0.5 (squares), 1.0 (diamonds), and 1.5 mM (stars) at a K8/K18 concentration of  $0.5 \text{ g l}^{-1}$ .

as time scale of the measurement, cross-link density, temperature, ionic strength, polymer length and protein concentration.

The  $\alpha$ -value of  $3/2$  observed in many experiments follows the predictions of the affine model, which derives the differential modulus from the entropic force required for the extension of a single semiflexible filament.<sup>11,39</sup> Theoretical considerations assuming a network of rigid rods with flexible cross-linkers such as filamin predict two scaling regimes with  $\alpha = 3/2$  at intermediate stresses and  $\alpha = 1$  at high stresses.<sup>44</sup> The latter is a result of the finite extensibility of the flexible cross-linkers. The

decreasing slope of the  $K'$  versus  $\sigma_0$  curves at high pre-stresses found for vimentin was attributed to stretching of the polymer backbone.<sup>12</sup> Another theoretical approach to describe the non-linear evolution of the differential modulus is the glassy wormlike chain model (GWLC).<sup>45–47</sup> This modification of the wormlike chain model includes an additional energy barrier  $\epsilon k_B T$ . The thermal relaxation of the filaments is hindered by additional short range attraction. According to the GWLC model the increase in  $K'$  and hence the  $\alpha$ -value strongly depend on the parameter  $\epsilon$ , which describes the stickiness of the filaments. For irreversibly cross-linked networks,  $\epsilon$  approaches infinity, which results in an  $\alpha$ -value of  $3/2$ . Lower values of  $\alpha$  correspond to weaker strength of bonds, which can break due to mechanical stress. The master curve in Fig. 10 indicates a universal strain stiffening mechanism with a finite  $\epsilon$  parameter within the framework of the GWLC model. The low  $\alpha$ -value and the decreasing slope of  $K'$  may be explained by a successive breaking of weak network bonds. The change in slope of the master curve at high pre-stresses might also originate from two different bond types with different strength of attractive interactions or from an extension of the individual filaments due to the high stresses prior to rupture. This latter hypothesis is supported by mechanical studies on single filaments of neurofilaments, desmin, and keratins 5 and 14. Accordingly, atomic force microscopy has revealed that IFs, *i.e.* keratins K5/K14 and desmin filaments as well as authentic neurofilaments, can be stretched up to threefold of their initial contour length before rupture.<sup>48</sup>

## Conclusions

We have investigated the linear and non-linear rheological properties of K8/K18 networks *in vitro* at different protein and  $\text{MgCl}_2$  concentrations. The linear viscoelastic behavior described by the frequency independent storage modulus  $G_0$  was obtained from small amplitude oscillatory shear. The non-linear response was characterized by LAOS and the differential modulus. The differential modulus  $K'$  was obtained from experiments superimposing a small oscillatory stress on a constant pre-stress. Experimental parameters were chosen such that artifacts from sample surface elasticity, wall slip or network formation within the rheometer gap were avoided. Even at protein concentrations as low as  $c = 0.1 \text{ g l}^{-1}$  an unexpected high frequency independent storage modulus  $G'$  is observed. Moreover,  $G_0$  depends only weakly on the protein concentration ( $G_0 \sim c^{0.5}$ ) and the critical deformation  $\gamma_{\text{crit}}$  at which the non-linear response sets in is independent of protein concentration. In analogy to the classical theory for swollen networks of flexible polymers, these findings can be rationalized assuming that the cross-link density decreases with decreasing IF concentration, but that the filament contour length between cross-links is independent of the protein concentration. Thus, filaments are more stretched at lower protein concentrations and accordingly the increase in conformational energy partly compensates the decrease in free energy related to the change of cross-link density. The predicted scaling of  $G_0 \sim c^{7/12}$  for a cross-linked network of flexible polymers swollen in a good solvent is in

excellent agreement with our experimental findings.  $G_0$  is independent of the  $\text{MgCl}_2$  concentration suggesting that the increased number of filament junctions revealed by electron microscopy goes along with a decreasing contribution of stretched filaments. Both effects balance and  $G_0$  remains constant. The changes in cross-link density due to  $\text{MgCl}_2$  appear not to be strong enough to be captured by the  $\gamma_{\text{crit}}$  measurements. The networks rupture when a critical strain  $\gamma_{\text{max}}$  is exceeded, but recovers and exhibits its initial viscoelastic response after a “healing” time of about 30 min. Other characteristic parameters of the non-linear network response are the stress  $\sigma_{\text{max}}$  at which the network ruptures and the corresponding modulus  $K'_{\text{max}}$ . These quantities strongly increase with increasing protein or  $\text{MgCl}_2$  concentrations. All data collapse onto a master curve when  $K'/G_0$  is plotted versus  $\sigma_0/\sigma_{\text{crit}}$ , where  $\sigma_{\text{crit}}$  is the stress at which non-linear response sets in. Two scaling regimes  $K' \sim \sigma_0$  are observed with  $\alpha \approx 1$  at intermediate stresses and  $\alpha \approx 0.6$  at high stresses. These scaling exponents are significantly lower than those predicted for permanently cross-linked networks of semiflexible filaments and may be rationalized within the framework of the GWLC model assuming sticky contacts with a finite and constant interaction parameter  $\varepsilon$ . The weak increase and the change in slope of  $K'$  are then a result of the successive failure of network bonds. The second regime with a lower slope of  $K'$  at high stresses could also be due to the existence of two types of sticky filament contacts with different bond energies or by the compliance of the individual filaments occurring at deformations. Further structural investigations on networks exposed to mechanical stresses are required to clarify this aspect.

## Acknowledgements

We acknowledge Tanja Lichtenstern (DKFZ) for technical assistance with the protein chemical procedures. Furthermore, we thank Ines Martin, Paul Walther and the staff at the electron micrograph facility at the University of Ulm for taking the electron micrographs. Norbert Mücke and Gijse Koenderink are thanked for helpful discussions. This work received support from the German Research Foundation, DFG (to HH: HE 1853/8-1).

## Notes and references

- H. Herrmann and U. Aebi, *Annu. Rev. Biochem.*, 2004, **73**, 749–789.
- E. Fuchs, *Annu. Rev. Cell Dev. Biol.*, 1995, **11**, 123–153.
- M. H. Lynch, W. M. O'Guin, C. Hardy, L. Mak and T. T. Sun, *J. Cell Biol.*, 1986, **103**, 2593–2606.
- M. Hatzfeld and K. Weber, *J. Cell Biol.*, 1990, **110**, 1199–1210.
- T. Lichtenstern, N. Mücke, U. Aebi, M. Mauermann and H. Herrmann, *J. Struct. Biol.*, 2012, **177**, 54–62.
- P. M. Steinert, *J. Biol. Chem.*, 1990, **265**, 8766–8774.
- K. E. Kasza, A. C. Rowat, J. Liu, T. E. Angelini, C. P. Brangwynne, G. H. Koenderink and D. A. Weitz, *Curr. Opin. Cell Biol.*, 2007, **19**, 101–107.
- N. Mücke, L. Kreplak, R. Kirmse, T. Wedig, H. Herrmann, U. Aebi and J. Langowski, *J. Mol. Biol.*, 2004, **335**, 1241–1250.
- F. Gittes, B. Mickey, J. Nettleton and J. Howard, *J. Cell Biol.*, 1993, **120**, 923–934.
- F. C. MacKintosh, J. Käs and P. A. Janmey, *Phys. Rev. Lett.*, 1995, **75**, 4425–4428.
- M. L. Gardel, J. H. Shin, F. C. MacKintosh, L. Mahadevan, P. Matsudaira and D. A. Weitz, *Science*, 2004, **304**, 1301–1305.
- Y.-C. Lin, N. Y. Yao, C. P. Broedersz, H. Herrmann, F. C. MacKintosh and D. A. Weitz, *Phys. Rev. Lett.*, 2010, **104**, 058101.
- Y.-C. Lin, C. P. Broedersz, A. C. Rowat, T. Wedig, H. Herrmann, F. C. MacKintosh and D. A. Weitz, *J. Mol. Biol.*, 2010, **399**, 637–644.
- H. Herrmann, T. Wedig, R. M. Porter, E. B. Lane and U. Aebi, *J. Struct. Biol.*, 2002, **137**, 82–96.
- S. Yamada, D. Wirtz and P. A. Coulombe, *J. Struct. Biol.*, 2003, **143**, 45–55.
- L. Ma, J. Xu, P. A. Coulombe and D. Wirtz, *J. Biol. Chem.*, 1999, **274**, 19145–19151.
- B. Hinner, M. Tempel, E. Sackmann, K. Kroy and E. Frey, *Phys. Rev. Lett.*, 1998, **81**, 2614–2617.
- K. Kroy and E. Frey, *Phys. Rev. Lett.*, 1996, **77**, 306–309.
- P. A. Janmey, U. Euteneuer, P. Traub and M. Schliwa, *J. Cell Biol.*, 1991, **113**, 155–160.
- M. Schopferer, H. Bär, B. Hochstein, S. Sharma, N. Mücke, H. Herrmann and N. Willenbacher, *J. Mol. Biol.*, 2009, **388**, 133–143.
- H. Bär, M. Schopferer, S. Sharma, B. Hochstein, N. Mücke, H. Herrmann and N. Willenbacher, *J. Mol. Biol.*, 2010, **397**, 1188–1198.
- O. I. Wagner, S. Rammensee, N. Korde, Q. Wen, J.-F. Leterrier and P. A. Janmey, *Exp. Cell Res.*, 2007, **313**, 2228–2235.
- S. Rammensee, P. A. Janmey and A. R. Bausch, *Eur. Biophys. J.*, 2007, **36**, 661–668.
- C. P. Broedersz, K. E. Kasza, L. M. Jawerth, S. Münster, D. A. Weitz and F. C. MacKintosh, *Soft Matter*, 2010, **6**, 4120–4127.
- H. Herrmann, M. Häner, M. Brettel, N.-O. Ku and U. Aebi, *J. Mol. Biol.*, 1999, **286**, 1403–1420.
- A. Leitner, T. Paust, O. Marti, P. Walther, H. Herrmann and M. Beil, *Biophys. J.*, 2012, **103**, 195–201.
- A. J. Kim, V. N. Manoharan and J. C. Crocker, *J. Am. Chem. Soc.*, 2005, **127**, 1592–1593.
- C. Oelschlaeger, N. Willenbacher and S. Nesar, *Prog. Colloid Polym. Sci.*, 2008, **134**, 74–79.
- M. T. Valentine, P. Kaplan, D. Thota, J. C. Crocker, T. Gisler, R. K. Prud'homme, M. Beck and D. A. Weitz, *Phys. Rev. E: Stat. Phys., Plasmas, Fluids, Relat. Interdiscip. Top.*, 2001, **64**, 15–17.
- W. K. Kegel and A. van Blaaderen, *Science*, 2000, **287**, 290–293.
- J. Appar, Y. Tseng, E. Fedorov, M. B. Herwig, S. C. Almo and D. Wirtz, *Biophys. J.*, 2000, **79**, 1095–1106.
- Y. Tseng and D. Wirtz, *Biophys. J.*, 2001, **81**, 1643–1656.
- P. A. Coulombe, O. Bousquet, L. Ma, S. Yamada and D. Wirtz, *Trends Cell Biol.*, 2000, **10**, 420–428.

- 34 M. L. Gardel, M. T. Valentine, J. C. Crocker, A. R. Bausch and D. A. Weitz, *Phys. Rev. Lett.*, 2003, **91**, 158302.
- 35 L. R. G. Treloar, *The physics of rubber elasticity*, Clarendon Pr., Oxford, 3rd edn, 2009.
- 36 M. Rubinstein and R. H. Colby, *Polymer Physics*, Oxford Univ. Pr., Oxford [u.a.], 1st edn, 2003.
- 37 F. Oppong, L. Rubatat, B. Frisken, A. Bailey and J. de Bruyn, *Phys. Rev. E: Stat. Phys., Plasmas, Fluids, Relat. Interdiscip. Top.*, 2006, **73**, 041405.
- 38 C. Storm, J. J. Pastore, F. C. MacKintosh, T. C. Lubensky and P. A. Janmey, *Nature*, 2005, **435**, 191–194.
- 39 M. L. Gardel, J. H. Shin, F. C. MacKintosh, L. Mahadevan, P. Matsudaira and D. A. Weitz, *Phys. Rev. Lett.*, 2004, **93**, 188102.
- 40 K. E. Kasza, G. H. Koenderink, Y.-C. Lin, C. P. Broedersz, W. Messner, F. Nakamura, T. P. Stossel, F. C. MacKintosh and D. A. Weitz, *Phys. Rev. E: Stat. Phys., Plasmas, Fluids, Relat. Interdiscip. Top.*, 2009, **79**, 041928.
- 41 C. Semmrich, T. Storz, J. Glaser, R. Merkel, A. R. Bausch and K. Kroy, *Proc. Natl. Acad. Sci. U. S. A.*, 2007, **104**, 20199–20203.
- 42 O. Lieleg and A. R. Bausch, *Phys. Rev. Lett.*, 2007, **99**, 158105.
- 43 R. Tharmann, M. M. A. E. Claessens and A. R. Bausch, *Phys. Rev. Lett.*, 2007, **98**, 088103.
- 44 C. P. Broedersz, C. Storm and F. C. MacKintosh, *Phys. Rev. Lett.*, 2008, **101**, 118103.
- 45 K. Kroy, *Soft Matter*, 2008, **4**, 2323–2330.
- 46 K. Kroy and J. Glaser, *New J. Phys.*, 2007, **9**, 416.
- 47 L. Wolff, P. Fernández and K. Kroy, *New J. Phys.*, 2010, **12**, 053024.
- 48 L. Kreplak, H. Bär, J.-F. Leterrier, H. Herrmann and U. Aebi, *J. Mol. Biol.*, 2005, **354**, 569–577.